Evaluation of Reanalysis Tropical Cyclone Structure with Global Hawk Dropsonde Observations

Alan Brammer, Chris Thorncroft

Department of Atmospheric And Environmental Science, University at Albany, State University of New York, Albany, New York

*

ABSTRACT

Tropical cyclone structure is evaluated from 3 reanalysis model grids with respect to over 2000 dropsondes from field campaigns during 2012-2016. Comparison with in-situ observations provides context for both research of tropical cyclones with reanalysis products as well the evaluation of tropical cyclone structures across different reanalysis products. This paper presents results from the National Center for Environmental Predictions (NCEP) Climate Forecast System Version 2 (CFSv2) as well as the European Center for Medium-Range Weather Forecasts (ECWMF) Reanalysis Interim (ERA-I) and Reanalysis 5 (ERA5). Thermodynamic and dynamic structures around the tropical cyclones are generally well represented in the reanalysis, though each reanalysis has it's own subtle bias. CFSv2 exhibits a shallow layer of negative temperature but positive moisture bias in the lower troposphere and a slight positive temperature bias at the top of the troposphere. ERA-I and ERA5 generally have low environmental biases though ERA5 has a slight dry bias along the top of the boundary layer. In the inner 100-200 km of the storms the magnitudes of the tropical cyclone warm-core and wind speeds are substantially underrepresented, though CFSv2 shows much better representation of the distributions compared to the older ERA-I but also better than the latest and higher resolution of ERA5. Although ERA5 has comparable warm-core magnitudes to CFSv2, the peak wind speeds throughout the troposphere remain around 20% too weak.

1. Introduction

Recent releases of large global high-resolution reanalysis datasets have enabled a wealth of research. These datasets are based on a combination of the available data assimilated into the system and the model cores integration of the atmospheric dynamics. These datasets are a great use for research into the large-scale influence of tropical cyclones (TCS;e.g Hart et al. 2007), however each have their own individual deficiencies in the representation of tropical cyclones (Schenkel and Hart 2012; Murakami 2014; Hodges et al. 2017) as well as the surrounding environment. Over the tropical oceans there are few in-situ observations and the vertical profile of measurements from satellites are restricted in vertical resolution therefore the assimilation schemes have relatively little data to work with. This also limits comparison of the reanalysis output to observations. The accuracy of the representation of cyclones, pre-genesis systems and the tropical atmosphere in general is not well documented currently mainly due to this lack of in-situ observations.

Understanding the limitations of how tropical cyclones of varying strengths are represented in the reanalysis is key for interpreting research which utilizes such data. Studies of tropical cyclone activity over time have found sensitivity to how tropical cyclones are defined and rely on choosing threshold values to closely match the observed record (Bengtsson et al. 2004, 2007; Hodges et al. 2017). Synoptic scale analysis with respect to tropical cyclones and TC genesis is also potentially influenced by the representation and structure of the TC. Over the Eastern Atlantic the low-level moisture profile has been shown to be a significant influence on the outcome of favourable African Easterly waves with respect to tropical cyclogenesis (Brammer and Thorncroft 2015; Schwendike et al. 2016). Understanding the limitations of reanalysis data around pre-genesis and existing tropical cyclones is therefore important to interpret results.

During 2012, 2013 and 2014, the NASA HS3 field campaign (Braun et al. 2016) flew an unmanned high-altitude drone (Global Hawk) over the Atlantic for a total of 670 hours during which time 1426 dropsondes were deployed from an altitude of approximately 18km ($\sim$ 50hPa). Follow on campaigns during 2015 & 2016 by the NOAA SHOUT program added another 741 dropsondes around tropical disturbances. These dropsondes in partner with remote sensing units on board generated detailed high-resolution profiles of the atmosphere across the tropics and around tropical storms during the campaign periods.

This paper will present a comparison of dropsondes with various current reanalysis products. Previous work has compared multiple reanalysis products with varying resolutions and dynamic cores, this work will therefore focus on differences between the NCEP Climate Forecast System (CFS) version 2 (CFSv2; Saha et al. 2014), which has been the realtime extension of the CFS Re-analysis (CFSR; Saha et al. 2010) since March 2011, with the European Center for Medium range Weather Forecasing (ECMWF) ERA-Interim (ERAI; Dee et al. 2011) and ECMWFs new ERA5 (Hersbach and Dee 2016) which is currently being released in stages during 2017-2019. This will provide insight into the biases of the thermodynamics and dynamics of the reanalysis products with respect to the tropical systems over the Atlantic.

2. Data and Methodology

Observational data were retrieved by the NASA HS3 and NOAA SHOUT field campaigns. these campaigns utilized the NCAR/NOAA dropsonde system launching miniature dropsondes from altitudes above 18km. The dropsondes measure pressure, dry-bulb temperature, relative humidity as well as wind-speed and direction. The RD94 dropsondes used in this campaign use the same pressure-temperature-humidity sensor as the Vaisala RS92 radiosonde, with documented high accuracy (e.g Nash et al. 2011; Intrieri et al. 2014). All dropsonde data has been quality-controlled using established post-processing methodology Wang et al. (2010) and has been reprocessed since the initial quality control released versions to correct for the dry bias that was present in the upper-troposphere (Young 2016).

Reanalysis dropsonde profiles were created through horizontal bicubic interpolation to the location of the dropsonde throughout the duration of the drop. Drops typically travel less than 20 km in the horizontal, which is currently less than the reanalysis grid spacing therefore there is minimal impact of whether launch, splash, or locations along the drop are used. Horizontal interpolation is performed for reanalysis time periods on either side of the drop time which are then linearly interpolated to the time of the drop. Dropsonde data are then extracted at the pressure levels of the reanalysis smoothing the data with a tolerance of $\pm$10 hPa.

Dropsonde storm relative locations were calculated with respect to HURDAT storm locations when a recorded system was being targeted. The HURDAT record was interpolated to the time of the drop (bicubic when possible, otherwise linear). Due to the potential error in the reanalysis storm centre locations, reanalysis storm relative profiles were calculated with respect to the center of the storm in the respective reanalysis grids, again interpolated to the time of the drop profile. Reanalysis storm centers were determined by nudging the HURDAT location to a combined mass weighted centre using MSLP, Relative Vorticity maxima at 925, 850 & 700 hPa as well as Geopotential height minima at 850 & 700 hPa similar to the GFDL tracking scheme (Marchok 2002). Further details and results using this technique are available in an online repository and in recent papers (Brammer 2017; Lin et al. 2017). For pre-invest or non-developing disturbances centers are determined as above in the reanalysis grids and dropsonde locations are calculated with respect to the mean of the location across the reanalysis datasets. Differences for both developed and non-developed disturbances across the reanalysis are typically less than 50 km similar to previous results (Schenkel and Hart 2012; Hodges et al. 2017).

The location of each dropsonde is plotted in Fig. 1, this shows that the drops were well spread across the Atlantic basin over the 5 years. The density of drops within 1000 km of a storm centre is also relatively well distributed across all directions (Fig. 2), beyond 1000 km from the storm center there is a slight increased number of drops in the North-West quadrant due to the typical flight path targeting Atlantic systems from the east coast of the USA.

3. Results

a. Mean Thermodynamic profile comparison

The vertical azimuthal mean structure of all targeted systems is presented in Fig. 3 for potential temperature (θ) and specific humidity anomalies measured by the dropsondes, variables have been subtracted from "environmental" drops ($\geq$ 350km from storm center) for all systems. The potential temperature anomalies show a strong upper level warm-core on average with mean anomalies from the environment of around 6 K between 500-200 hPa. The standard deviation of potential temperature is also maximised in the inner core and in the upper-troposphere. Specific humidity anomalies show a peak in moisture anomaly around 700 hPa in the inner 100 km of the systems. As this figure includes systems from pre-genesis to hurricane strength there is large variability not captured. This will be addressed in later figures, Doyle et al. (2017) also analysed the warm-core profile and relationship to storm structure as measured by the HS3 drops in more detail. These mean structures however provide a reference for evaluating the reanalysis models.

Figure 4 shows the bias or mean anomaly between each dropsonde and the profile extracted from the reanalysis grids which are then binned to respective model storm relative coordinates. For all 3 reanalysis grids the warm-core anomaly has a large negative temperature bias in the inner 100-200 km of the tropical systems. CFSv2 also exhibits a cold bias extending uniformly out from the storm centre between 950 and 700 hPa peaking at over 1 K from 700 to 1200 km from the storm centre. The standard deviation of anomalies throughout this region is approximately equal to the mean bias suggesting that the most of the distribution of temperatures throughout this layer are substantially warmer in reality than represented in the reanalysis. Coincident with this cold bias in the CFSv2, there is also a positive moisture bias (Fig. 4b) although the mean anomaly peaks at 0.3 g kg^{-1} while the standard deviation of anomalies is around 1.4 g kg^{-1}. At upper levels CFSv2 also shows a small positive temperature bias on a vertical gradient of increasing standard deviation. This upper level bias however is relatively small with respect to the standard deviation of anomalies.

Both ERAI and ERA5 show similar temperature biases (Fig. 4c,e), with substantial negative bias in the inner core of the storms but generally weak to no bias outside of the inner 200 km. The magnitude and extent of the negative bias within in inner core is most notable for ERAI but the horizontal resolution of this reanalysis is the lowest. As well as the inner-core negative temperature bias, ERAI also shows a substantial dry bias in the inner 100 km of the storm, although this once again can likely be attributed to the lower resolution. ERA5 shows a smaller region of negative temperature bias around the inner-core, showing that with the increased horizontal resolution the model has improved around the inner 50-150km. Beyond 500 km ERA5 shows a dry bias in the lower troposphere maximised at 850 hPa but extending up to 700 hPa at larger radii. CFSv2 also exhibits a dry boundary layer bias below the lower-troposphere positive bias, suggesting reasonable uncertainty between the reanalysis products for low level moisture, the depth of the boundary layer and shallow convection schemes. The vertical resolution of the reanalysis grids likely also plays into the representation of variability in these lowest levels, the dropsondes are extracted relative to the reanalysis grid levels but will still retain higher variability signals.

b. Mean Dynamic profile comparison

The mean profile of total wind magnitude and the tangential and radial components measured by the dropsondes are shown in (Fig. 5). The dropsondes show the inner core wind maxima with winds peaking near 25 ms^{-1} in the lower troposphere in the inner 50 km bin around 925 hPa with a wind maxima extending out at this level. At upper levels a large anticyclone is evident with tangential and radial flow maxima overlapping at 200 hPa and 700-1000 km from the storm center. Low-level radial inflow is restricted between the surface and 850 hPa from around 700-900 km to the center and with a mean inflow up to 4 ms^{-1}.

The reanalysis bias for both tangential and radial flow is shown in Fig. 6. As expected tangential flow in the inner 100 km is substantially weaker than observed across the three reanalyses. For CFSv2 (Fig. 6a) this weak bias is restricted to the inner 100 km with less than 1 ms^{-1} error beyond 150 km in the lower troposphere. Given coarser resolution of ERAI it is not surprising that the weak bias extends further from the center of the storms. It is interesting to note that the peak tangential wind of 14 ms^{-1} in ERAI however occurs approximately 200 km from the storm center (Fig. 6c). This result aligns with the results presented in Hodges et al. (2017) wherein the authors showed that ERAI wind maxima was at a radius approximately double the observed RMW compared to 1.25x for the CFSv2. ERA5 shows a similar mean structure to CFSv2 with tangential wind maxima approximately 100-200 km from the center, though the mean composite peaks at 12 ms^{-1} which is 2 ms^{-1} weaker than both CFSv2 and ERAI. This negative anomaly for tangential wind also extends out beyond 500 km as well, showing that the large scale circulation around the ERA5 storms are weaker than observed over a large area. For radial flow all three reanalyses exhibit similar bias with weak radial inflow in the boundary layer, the inflow is approximately half the magnitude of that observed. Generally the structure of the upper level outflow is resolved well with peak outflow between 700-900 km from the storm center, however the outflow over the storm is too weak coincident with tangential flow that is also too strong in the inner 200 km. Therefore although the storm is generally too weak in the lower troposphere the cyclonic vortex is also too strong in the upper levels, i.e. the vertical gradient of vorticity is not resolved sufficiently.

c. Distribution of Storm Characteristics

The previous section has shown that while reanalyses can represent the large scale structure (250+km from the center) of tropical cyclones there are substantial issues in the inner 250 km of the systems. This is largely unsurprising given the resolution of the models, however given the use of long-term reanalysis products in tropical cyclone related studies it is important to document the extent of the limitations. This section will present distribution storm-scale characteristics for different categories of cyclone strength.

Figure 7 shows the upper and lower quartiles of potential temperature anomalies for systems tropical depression or weaker (referred to just as TD hereafter), tropical storm (TS) and hurricane (HU) according to HURDAT. For both TD and TS strength systems, the relatively weak warm-core structures of less than 4-5 K are resolved well by the reanalysis models with the upper and lower quartiles approximately equal throughout the profile. For the TD category however (Fig. 7a), all 3 reanalyses underestimate the lower tropospheric warm-core between 900-600 hPa. For tropical storms, the reanalyses show a better agreement with the dropsondes throughout the profile, though the upper quartiles for the warm-core at 300 hPa starts to display a slight cold bias (0.5-1 K) for CFSv2 and ERAI. Once the tropical cyclones reach hurricane strength the inability of the reanalysis products to resolve the gradients associated with a strong warm-core becomes evident. At the lowest horizontal resolution, ERAI has the weakest warms cores with upper-quartile of warm-core anomalies at 300 hPa only 1 K above the lower-quartile of observed warm-core anomalies and

4 K below the respective observations. Although ERAI does show a maximum in the distribution around 300 hPa the lower troposphere exhibits almost a constant vertical profile of θ anomalies between 0-2 K. Both CFSv2 and ERA5 show a better vertical profile with increasing θ anomalies from the surface to a maximum around 300 hPa. Both models fail to resolve the magnitude of the upper-level warm-core however with the upper quartile between 6-7 K while the upper quartile of the dropsondes have values of around 9 K. For both TS and HU categories it is interesting to note that CFSv2 tends to have a small (0.5-1 K) positive bias of lower tropospheric θ anomalies at the lower quartile of the distribution.

The distribution of wind magnitudes per strength category is presented in Fig. 8. Similar to the thermodynamic structure the weak winds associated with TDs are well captured by the reanalysis grids with the upper and lower quartiles equivalent throughout the troposphere (Fig. 8a). For TS and HU strength systems however the substantial weak bias across the distribution of systems becomes clear. For tropical storms, CFSv2 has the strongest upper quartile of winds throughout the profile but is still underestimating compared with the dropsondes by around 5 ms^{-1}. ERA5 and ERAI have similar distributions throughout the profile both underestimating the upper quartile of wind strengths by around 10 ms^{-1}. Given the increased horizontal resolution and thermodynamic profiles it is surprising that the distribution of wind speeds from ERA5 are comparable to ERAI. For hurricane strength systems, the reanalyses have a substantial weak bias for the whole distribution of wind speeds throughout the profile. Throughout the lower troposphere (1000-400 hPa) ERAI and ERA5 upper-quartile of wind speeds are within 2-5 ms^{-1} of the lower quartile of dropsonde wind speeds. Similar to tropical storm strength systems, ERA5 is very similar to ERAI with just a small increase across the distribution of 2-5 ms^{-1}. CFSv2 has the closest representation to the dropsondes throughout the vertical profile with a wind speed maximum around 900 hPa, though the upper and lower quartiles are still around 10 ms^{-1} too weak throughout the profile.

Figure 9 shows how the maximum wind per dropsonde profile correlates to the maximum wind derived from the reanalysis grids with marker colour representing the distance from the storm center. Across all three reanalyses it is clear that wind speed maxima at greater radii have better correlation with observations falling closer to the x=y line. For CFSv2 profiles at the larger radii (100+ km) fall close to x=y line even for wind speeds around 50 ms^{-1} (Figure 9a), whereas both ERAI and ERA5 show a consistent weak bias for all profiles with points consistently falling below the x=y line. This highlights the previous results showing that for ERAI and ERA5 the weak wind speeds are not directly related to either wind speed strength or the resolution of the inner core of the system. To highlight the varying correlation coefficients across different radii, Figure 10 shows both the correlation and regression slope (β) between model and observed wind speeds throughout the troposphere for the 3 strength categories. Ideally both the correlation and β would be close to 1.

Correlation between reanalysis and dropsonde wind speed is generally lowest across all radial bins out to 900+ km for TD or weaker disturbances (Fig 10a). ERA5 and ERAI both have substantially better correlation coefficients (0.8-0.9) than CFSv2 (0.7) for this relatively normal tropical atmosphere. This suggests that while CFSv2 is resolving appropriate distribution of wind speeds and θ anomalies the structure of these may be inconsistent with respect to observations. At this strength CFSv2 does not relocate the vortex, due to a lack of observations and center fixes. For tropical storms and hurricanes the environmental winds are much better correlated with coefficients tending towards 0.95 in the outer radii. Correlation drops slightly for wind-speeds in the inner 100 km of tropical storms though remains above 0.6 for all 3 reanalysis (Fig 10b). While for hurricanes the impact of horizontal resolution becomes evident with correlation falling to less than 0.4 for CFSv2 and ERAI in the inner 50 km. ERA5 remains relatively high, considering the significant weak bias in wind speeds. The well defined structure of the hurricane means that

CFSv2 has better correlation at 100 km for a hurricane wind speeds than at 200 km for a TD. This highlights that while the inner core of strong systems is poorly resolved, the reanalysis models can resolve the winds once past 2-3 times their grid scale. Though the poor correlation for tropical depression and weaker systems suggests that these disturbance are not well represented in the reanalysis currently.

The distribution of wind-speeds for both the inner 250 km radii and all drops outside of 250 km are shown in Figure 11. This highlights nicely the disparity between the ability for reanalysis products to capture the increased wind-speeds or strong gradients around the center of tropical cyclones against the better representation on the large scale. For profiles outside of tropical cyclone the distribution of wind-speeds are generally very close to observed, although the weak bias of ERA5 is evident for wind-speeds above 18 ms^{-1}. Although the reanalysis products attain 30 ms^{-1} at a correct frequency outside the tropical cyclone, once inside inner 100-200 km of the storm all 3 reanalysis products show a substantial shift of the distribution to lower wind speeds.

4. Conclusions

Previous literature has compared the differences in both reanalysis TC structure (Schenkel and Hart 2012), occurrence (Hodges et al. 2017) as well as outer wind field size (Lin et al. 2017). These studies are typically somewhat limited by the observations utilised either relying solely on the recorded intensity of the tropical cyclone or matching surface winds at large radii. Given the wealth of data collected by the global hawk during the HS3 field campaign and subsequently with the SHOUT campaigns, this evaluation of reanalysis storm structure has aimed to document the abilities and limitations of these long term reanalysis products for both inner core intensity and outer wind field representation.

This comparison of over 2500 hundred dropsondes with profiles extracted from reanalysis grids highlights the biases associated with gridded fields around tropical cyclones. As expected reanalysis grids struggle to resolve inner core magnitudes for both dynamic and thermodynamic fields. Both CFSv2 and ERA5 have lower biases when compared to the coarser resolution of ERAI. However, ERA5 does not show a substantial improvement over CFSv2 given that ERA5 also has a substantially improved horizontal resolution. CFSv2 has been shown to perform better than other reanalysis for storm center characteristics in the past arguably attributed to the vortex relocation employed (Schenkel and Hart 2012; Hodges et al. 2017). While this method has been shown to have issues it does seem to still aid in reproducing inner core and near-by environmental structure when compared to the higher resolution ERA5 reanalysis.

The improved resolution of ERA5 and CFSv2 gives a clear improvement compared to the coarser ERAI for the representation of both wind speeds and thermodynamic profiles for tropical storms and hurricanes although both still underestimate intensity. It is also important to consider that these weak biases extend from the center of the disturbances out to 100-200 km from the center and throughout the troposphere as well.

While CFSv2 may have slightly better representation of the wind field, outside the inner core there is a substantial cold bias throughout the lower troposphere. In the transition from CFSR to CFSv2 changes were made to the shallow convection scheme to improve the stratus deck over the south eastern Pacific (Sun et al. 2010; Saha et al. 2014), while all the results presented here are for after that change was implemented, it seems likely that these changes have now resulted in an over active shallow convection scheme for the Atlantic basin creating this cool and slightly moist layer.

Analysis of the correlation of wind-speeds across tropical cyclone strength showed that Tropical Depressions and weaker typically have lower correlation than stronger systems. This could be in part due to the synoptic forcing of a tropical cyclone on the surrounding environment but also could be due to increased observations and assimilation of data around tropical storms. This result in part highlights a need to both observe pre-genesis and weak disturbances to provide assimilation schemes with data but also suggests that analysis of weak disturbances be corroborated across different reanalysis products.

This evaluation and comparison with deep tropospheric dropsonde measurements has shown that while the reanalysis grids have deficiencies in magnitude of tropical storms. Generally the biases are small (≤ 1 K) and outside of the inner 200 km of the storm less than 1 ms^{-1}. These biases should be taken into consideration when using reanalysis for tropical cyclone research especially analysis that integrates these biases over time (e.g. trajectories within 200 km of a storm). Given the weak bias in wind speeds shown here and previously by Hodges et al. (2017), the full tropospheric dropsonde measurements could provide a large dataset to bias-correct inner core wind speeds for improved tropical cyclone intensity forecasting from the coarse resolution global models.

References

Bengtsson, L., S. Hagemann, and K. I. Hodges, 2004: Can climate trends be calculated from reanalysis data? *J. Geophys. Res.: Atmos.*, **109 (D11)**, 1130.

Bengtsson, L., K. Hodges, and M. ESCH, 2007: Tropical cyclones in a T159 resolution global climate model: comparison with observations and re-analyses. *Tellus A*, **59 (4)**, 396–416.

Brammer, A., 2017: Multivariable Tropical Cyclone Vortex Tracker in NCL. Zenodo. http://doi.org/10.5281/zenodo.266194.

Brammer, A., and C. D. Thorncroft, 2015: Variability and Evolution of African Easterly Wave Structures and Their Relationship with Tropical Cyclogenesis over the Eastern Atlantic. *Mon. Wea. Rev.*, **143 (12)**, 4975–4995.

Braun, S. A., P. A. Newman, and G. M. Heymsfield, 2016: NASA's Hurricane and Severe Storm Sentinel (HS3) Investigation. *Bull. Amer. Meteor. Soc.*, **97 (11)**, 2085–2102.

Dee, D. P., and Coauthors, 2011: The ERA-Interim reanalysis: configuration and performance of the data assimilation system. *Q. J. R. Meteorol. Soc.*, **137 (656)**, 553–597.

Doyle, J. D., W. A. Komaromi, and J. D. Doyle, 2017: Tropical Cyclone Outflow and Warm Core Structure as Revealed by HS3 Dropsonde Data. *Mon. Wea. Rev.*, **145 (4)**, 1339–1359.

Hart, R. E., R. N. Maue, and M. C. Watson, 2007: Estimating local memory of tropical cyclones through MPI anomaly evolution. *Mon. Wea. Rev.*, **135 (12)**, 3990–4005.

Hersbach, H., and D. P. Dee, 2016: ERA5 Reanalysis is in Production. *ECMWF Newsletter*, **(Spring)**.

Hodges, K., A. Cobb, and P. L. Vidale, 2017: How Well Are Tropical Cyclones Represented in Reanalysis Datasets? *J. Clim.*, **30 (14)**, 5243–5264.

Intrieri, J. M., and Coauthors, 2014: Global Hawk dropsonde observations of the Arctic atmosphere during the Winter Storms and Pacific Atmospheric Rivers (WISPAR) field campaign. *Atmospheric Measurement Techniques Discussions*, **7 (4)**, 3917–3926.

Lin, N., D. Chavas, M. Oppenheimer, B. A. Schenkel, and A. Brammer, 2017: Evaluating Outer Tropical Cyclone Size in Reanalysis Datasets Using QuikSCAT Data. *J. Clim.*, **30 (21)**, 8745–8762.

Marchok, T. P., 2002: How the NCEP tropical cyclone tracker works. *25th Conf. on Hurricanes and Tropical Meteorology, San Diego, CA, Amer. Meteor. Soc.*, 21–22.

Murakami, H., 2014: Tropical cyclones in reanalysis data sets. *Geophys. Res. Lett.*, **41 (6)**, 2133–2141.

Nash, J., T. Oakley, H. Vomel, and W. Li, 2011: WMO Intercomparisons of high quality radiosonde system. URL http://www.wmo.int/pages/prog/www/IMOP/publications/IOM-107_Yangjiang.pdf.

Saha, S., and Coauthors, 2010: The NCEP Climate Forecast System Reanalysis. *Bull. Amer. Meteor. Soc.*, **91 (8)**, 1015–1057.

Saha, S., and Coauthors, 2014: The NCEP Climate Forecast System Version 2. *J. Clim.*, **27 (6)**, 2185–2208.

Schenkel, B. A., and R. E. Hart, 2012: An examination of tropical cyclone position, intensity, and intensity life cycle within atmospheric reanalysis datasets. *J. Clim.*, **25 (10)**, 3453–3475.

Schwendike, J., S. C. Jones, B. Vogel, and H. Vogel, 2016: Mineral Dust Transport towards Hurricane Helene (2006). *J. Geophys. Res.: Atmos.*, **121**.

Sun, R., S. Moorthi, H. Xiao, and C. R. Mechoso, 2010: Simulation of low clouds in the Southeast Pacific by the NCEP GFS: sensitivity to vertical mixing. *Atmospheric Chemistry and Physics*, **10 (24)**, 12 261–12 272.

Wang, J., and Coauthors, 2010: Water vapor variability and comparisons in the subtropical Pacific from The Observing System Research and Predictability Experiment-Pacific Asian Regional Campaign (T-PARC) Driftsonde, Constellation Observing System for Meteorology, Ionosphere, and Climate (COSMIC), and reanalyses. *J. Geophys. Res.*, **115 (D21)**, D21 108.

Young, K., 2016: NCAR/EOL Technical Note Dropsonde Dry Bias . URL https://www.eol.ucar.edu/system/files/software/Aspen/Windows/W7/documents/Tech%20Note%20Dropsonde_Dry_Bias_20160527_v1.3.pdf.

LIST OF FIGURES

Fig. 1. Location of each dropsonde. Colors correspond to the horizontal distance from the center of nearest tropical system. 19

Fig. 2. Storm Relative Dropsonde Distribution. 20

Fig. 3. Mean θ and specific humidity for all dropsondes from 2012-2016 in storm relative coordinates. Shading shows anomaly from the mean environmental (300+km) conditions. Contours show the standard deviation. 21

Fig. 4. Mean θ and specific humidity for all dropsondes from 2012-2016 in storm relative coordinates. Shading shows anomaly from the dropsondes. Contours show the standard deviation of the anomalies. 22

Fig. 5. Mean total wind speed (a) and tangential and radial components of wind (b) for all dropsondes from 2012-2016 in storm relative coordinates. (b) shading shows tangential component, contours show radial flow. 23

Fig. 6. Reanalysis bias for tangential (a,c,d) and radial (b,d,f) azimuthal mean plots for all targeted systems. Shading shows anomaly from the dropsondes. Contours show the reanalysis mean for each respective field. 24

Fig. 7. Quartile ranges of warm-core anomalies from drops and profiles for each reanalysis grid for TD or weaker, TS and Hurricane strength systems. 25

Fig. 8. Quartile ranges of wind speeds from drops and profiles for each reanalysis grid for TD or weaker, TS and Hurricane strength systems in the inner 250 km of systems. 26

Fig. 9. Scatter plot of maximum wind per drop profile from CFSv2 (a), ERAI (b) and ERA5 (c) for drops within 250 km of the storm center. Color of markers indicates distance from storm. . . . 27

Fig. 10. Correlation of wind speed for drops per radial distance from the storm center for TD (left), TS (middle) & Hurricane (right) strength systems. Radial bins are designated such that there are 50 drops per bin. Due to fewer flights into weak disturbances the TD figures have fewer radial bins. 28

Fig. 11. Distribution of wind speed maxima for inner core and environmental drops. 29

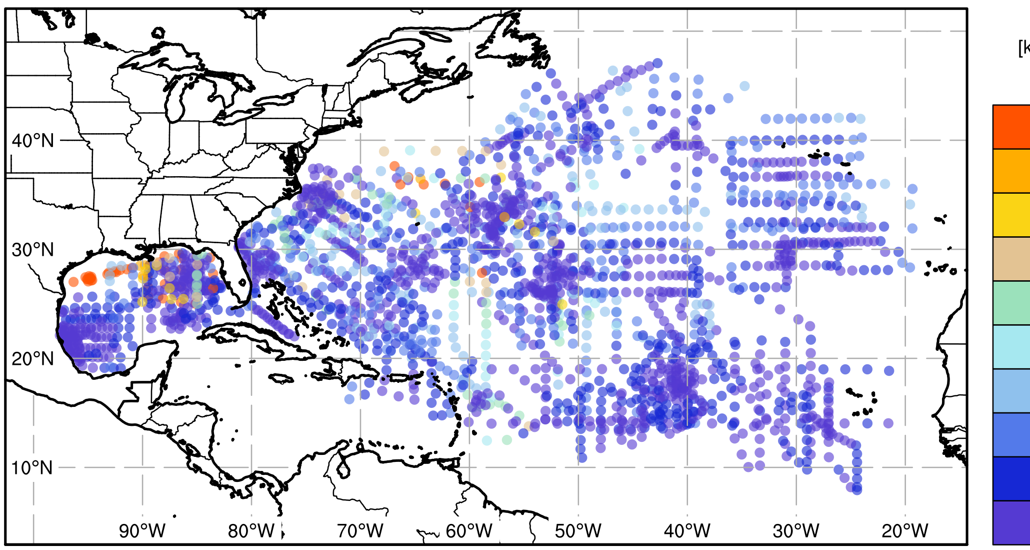

378 FIG. 1. Location of each dropsonde. Colors correspond to the horizontal distance from the center of nearest
379 tropical system.

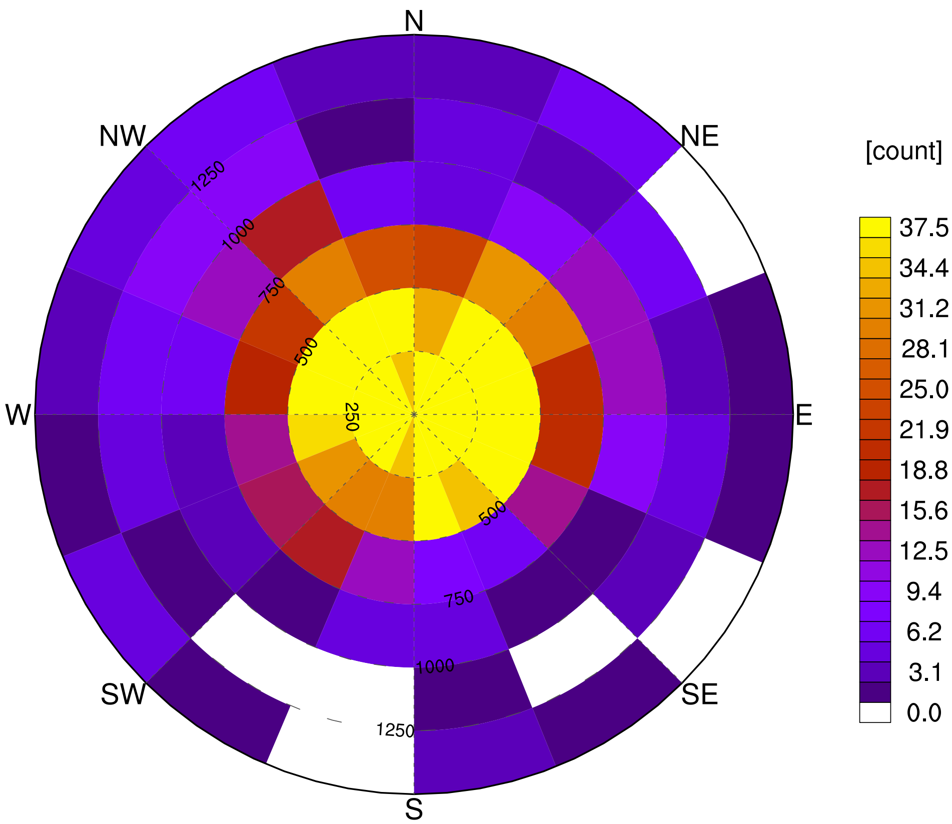

FIG. 2. Storm Relative Dropsonde Distribution.

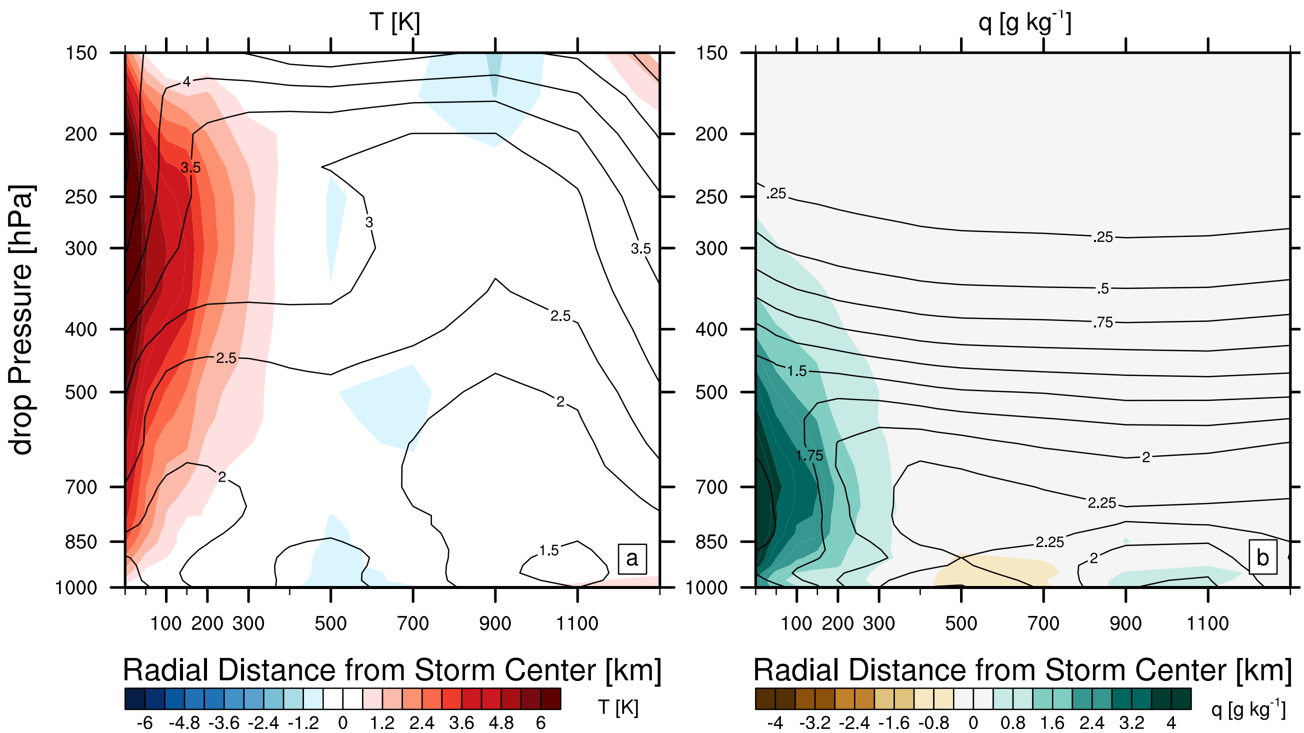

380 FIG. 3. Mean θ and specific humidity for all dropsondes from 2012-2016 in storm relative coordinates. Shading shows anomaly from the mean environmental (300+km) conditions. Contours show the standard deviation.

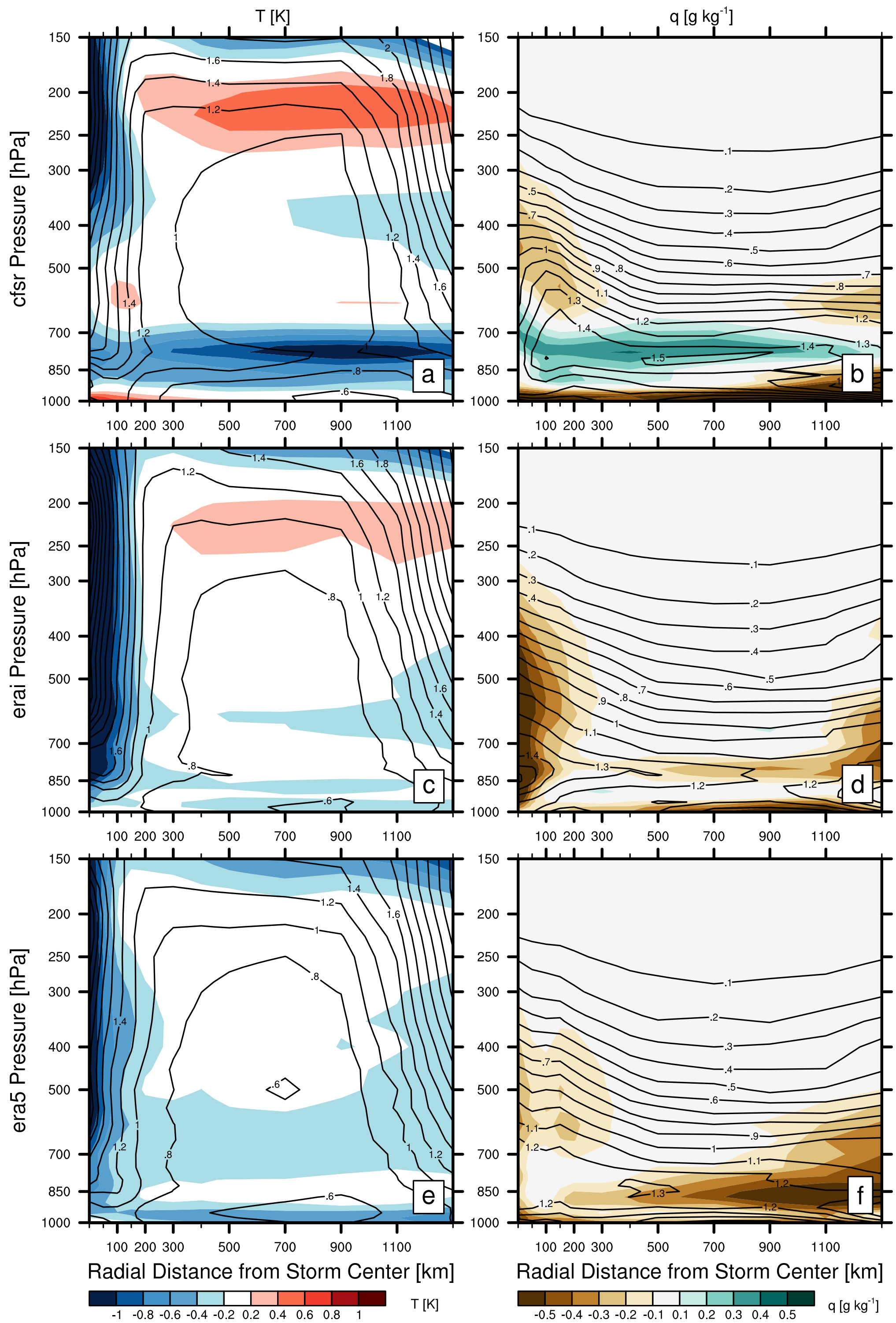

382 FIG. 4. Mean θ and specific humidity for all dropsondes from 2012-2016 in storm relative coordinates.
383 Shading shows anomaly from the dropsondes. Contours show the standard deviation of the anomalies.

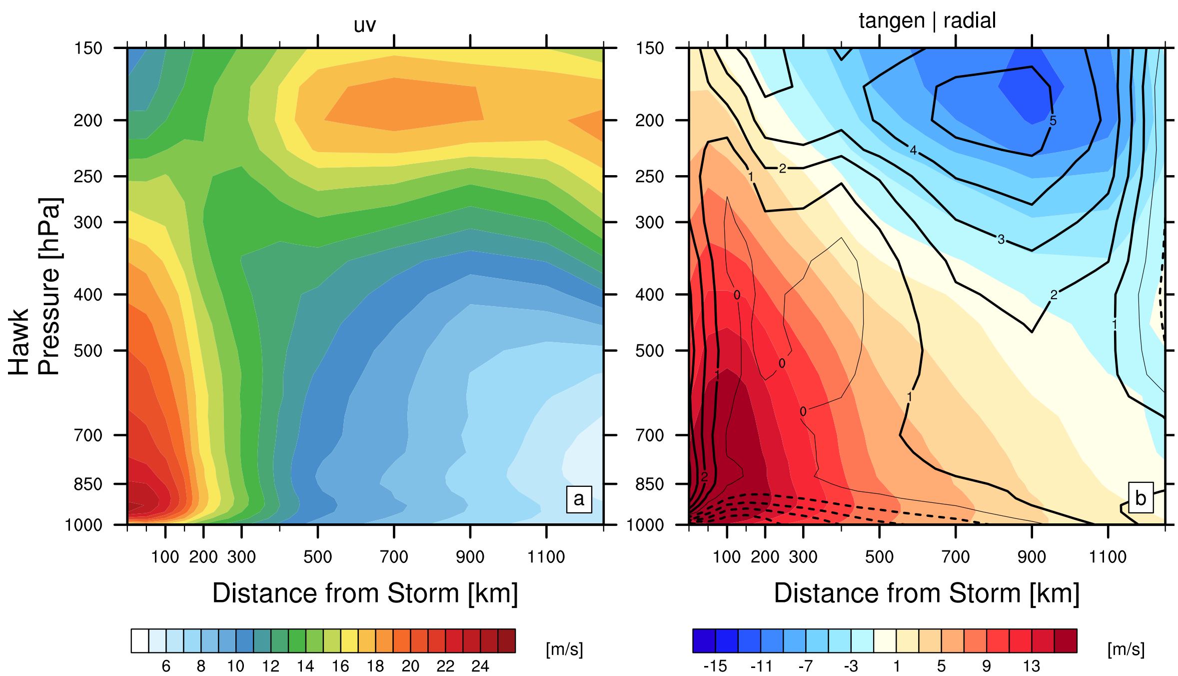

FIG. 5. Mean total wind speed (a) and tangential and radial components of wind (b) for all dropsondes from 2012-2016 in storm relative coordinates. (b) shading shows tangential component, contours show radial flow.

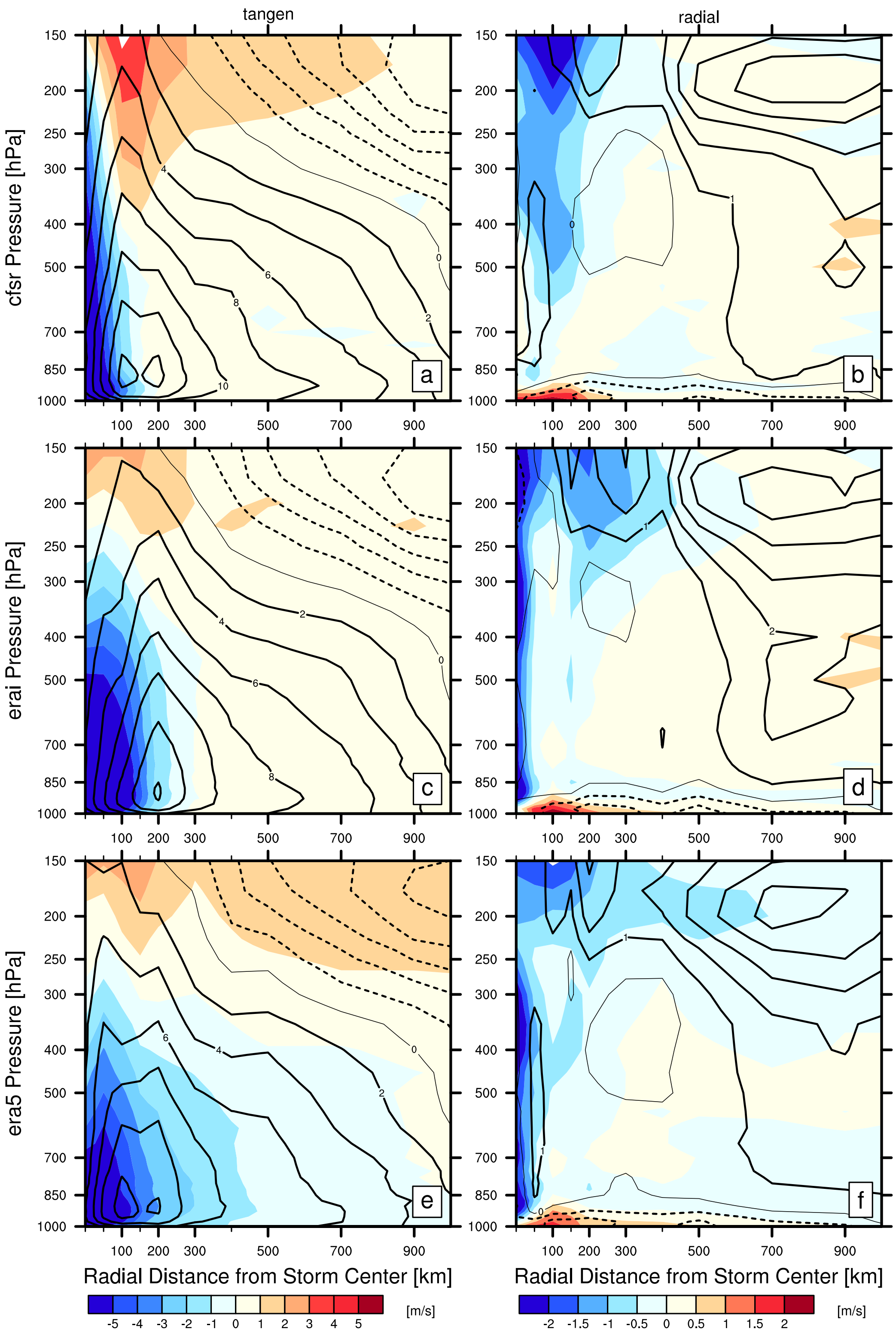

FIG. 6. Reanalysis bias for tangential (a,c,d) and radial (b,d,f) azimuthal mean plots for all targeted systems. Shading shows anomaly from the dropsondes. Contours show the reanalysis mean for each respective field.

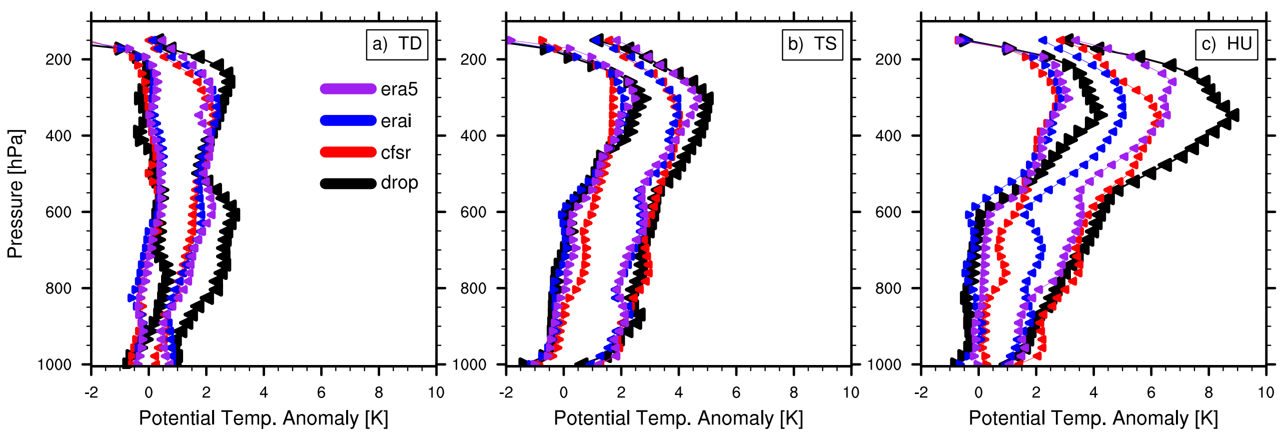

388 FIG. 7. Quartile ranges of warm-core anomalies from drops and profiles for each reanalysis grid for TD or
389 weaker, TS and Hurricane strength systems.

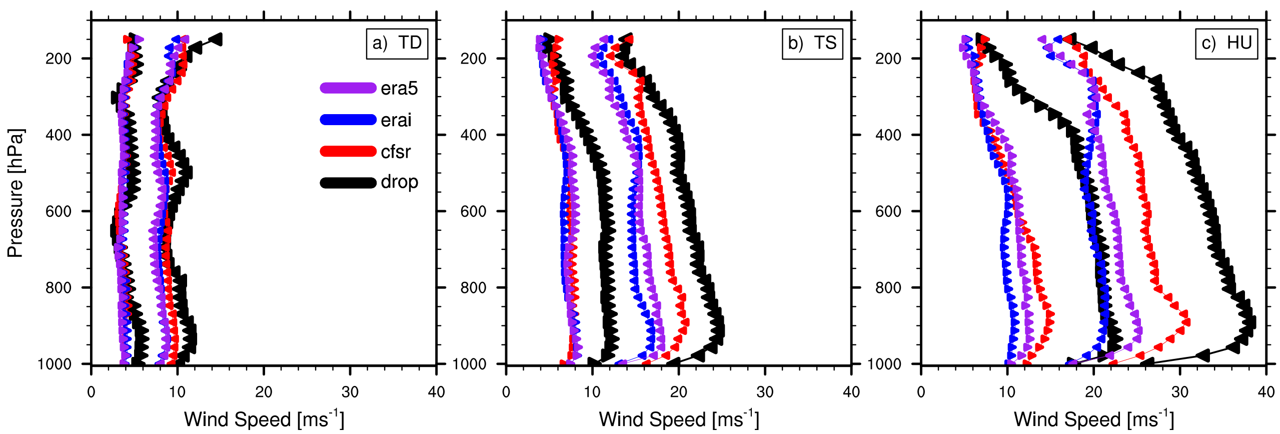

390 FIG. 8. Quartile ranges of wind speeds from drops and profiles for each reanalysis grid for TD or weaker, TS
391 and Hurricane strength systems in the inner 250 km of systems.

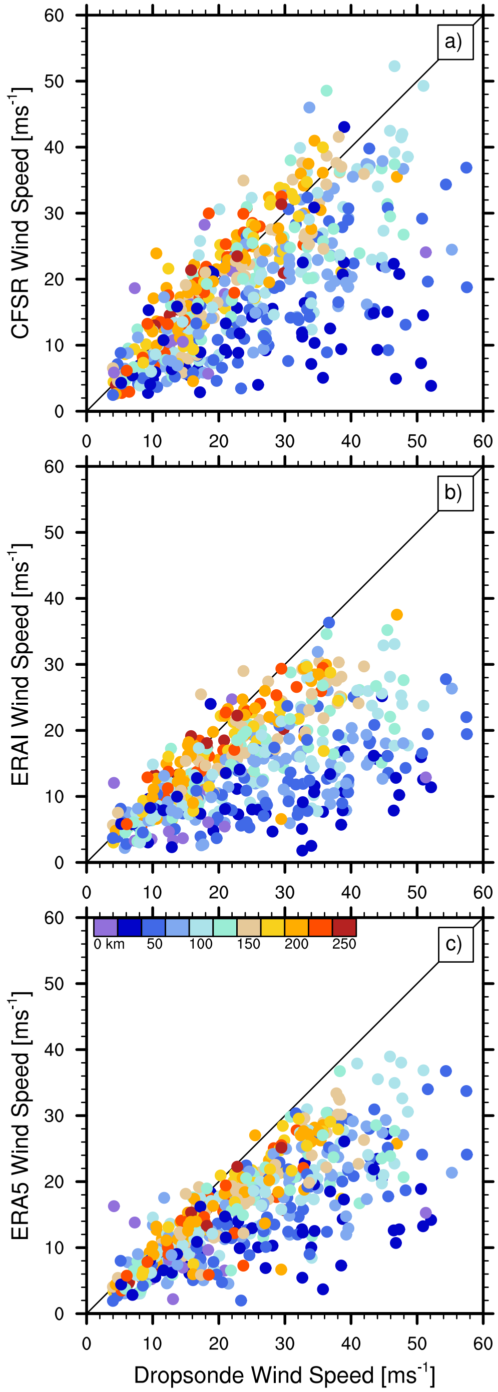

FIG. 9. Scatter plot of maximum wind per drop profile from CFSv2 (a), ERAI (b) and ERA5 (c) for drops within 250 km of the storm center. Color of markers indicates distance from storm.

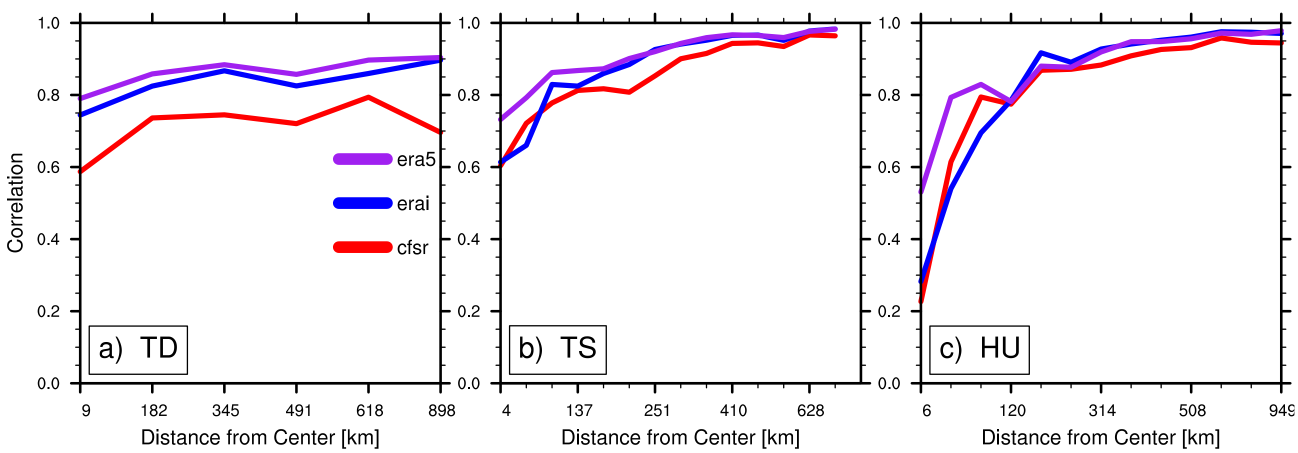

FIG. 10. Correlation of wind speed for drops per radial distance from the storm center for TD (left), TS (middle) & Hurricane (right) strength systems. Radial bins are designated such that there are 50 drops per bin. Due to fewer flights into weak disturbances the TD figures have fewer radial bins.

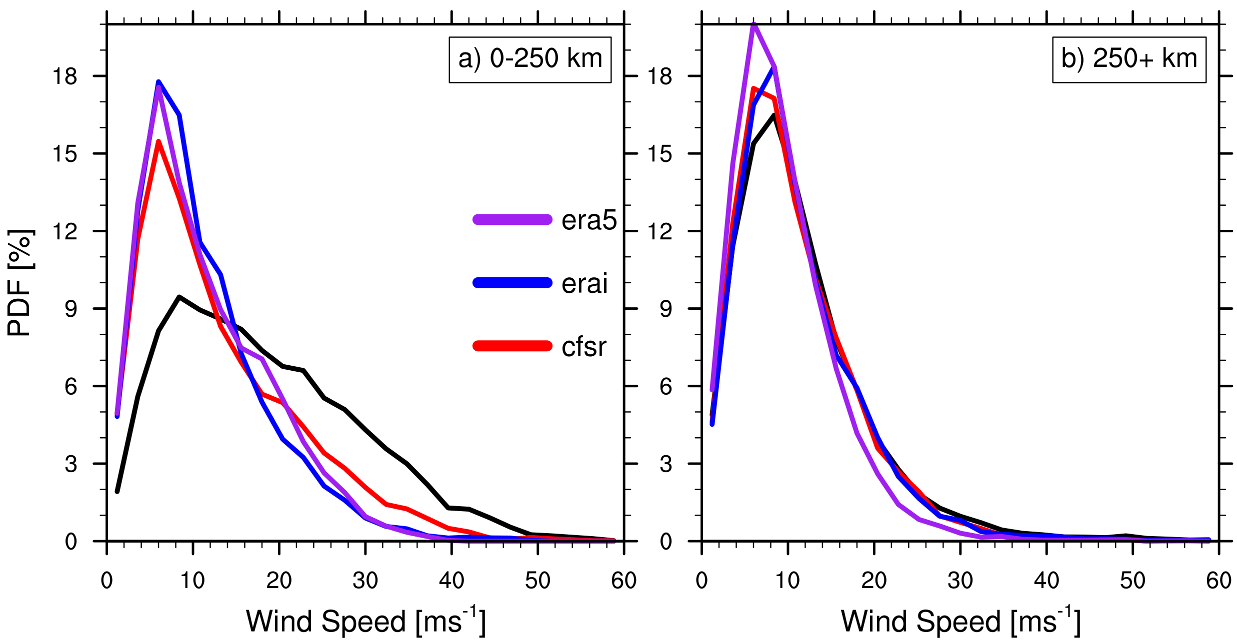

FIG. 11. Distribution of wind speed maxima for inner core and environmental drops.